Loss-Minimization Strategy of Nonsinusoidal Back EMF PMSM in Multiple Synchronous Reference Frames

Haitao Zhang, Manfeng Dou, *Member, IEEE*, and Jia Deng

***Abstract*—Traditional loss-minimization strategies of model-based control, copper loss minimization (CLM), and finite-element-based control suffer from respective problems of iron loss mismatch with a physical view, pseudominimization and amounts of efforts when they are applied to permanent magnet synchronous motor with nonsinusoidal back electromotive force (NS-PMSM). This article combines theories of multiple synchronous reference frames and iron loss resistance to develop a new model of NS-PMSM, based on which the stator iron loss is evaluated to match well with the physical view. Then, a current strategy is proposed to minimize the total stator loss under constraints of ripple-free torque and finite dc supply. The optimal current solution is solved in closed form and implemented effortlessly. A good robustness to phase resistance variation is also achieved. Compared to CLM, the proposed strategy realizes a true minimization with the stator loss reduced by 9% and the motor efficiency enhanced by 0.7% at rated operation of a 3.8-kW NS-PMSM. Precision of the iron loss evaluation and performances of the strategy are validated experimentally on the 3.8-kW motor setup.**

***Index Terms*—Iron loss evaluation, loss minimization, multiple synchronous reference frames (MSRF), nonsinusoidal back electromotive force (EMF), permanent magnet synchronous motor (PMSM).**

I. Introduction

PERMANENT magnet synchronous motor (PMSM) with surface-mounted magnets is attracting growing attentions in drive systems of aerospace applications, owing to its advantages of high power density and simple structure [1]–[3]. In these applications, a shortage of power energy is probably suffered due to finite chemical fuels or solar cells. Concerning the motor usually consumes most of the power in the whole system, it is eagerly expected to reduce the motor loss as much as possible to save the power energy.

Recent years, in addition to design schemes, many control strategies have been proposed to reduce the loss of PMSM. They are developed in single synchronous rotary frame (SRF1), and according to the underlying principles, can be divided into three categories of model-based control, copper loss minimization (CLM), and finite-element (FE)-based control.

In the model-based control, additional d-axis current is injected into the motor to weaken the airgap field, then flux densities in stator teeth and yokes are reduced, leading to a less stator iron loss. Though the copper loss is increased, the sum of the two losses is reduced. In this strategy, an iron loss resistance theory is developed with a virtual resistance inserted in parallel with magnetizing branches of d- and q-axis circuits, so that the iron loss is evaluated as ohmic power of the resistance [4], [5]. Then, the optimal current solution can be determined. Moreover, an iron loss torque caused by hysteresis and eddy-current effects of the stator core is properly compensated. In literature [6]–[8], the model-based strategy was implemented incorporating the field-orientated control, predictive torque control, and direct torque flux control, respectively, so that high motor efficiency and fast torque response were achieved simultaneously. However, a problem for the strategy is that the stator iron loss is modeled in SRF1 with only sinusoidal current and back electromotive force (EMF) considered. In aerospace applications, the PMSMs are usually designed with radially magnetized magnets to strengthen the rotor fundamental magnetic field to achieve a higher power density, and with concentrated windings to reduce the winding ends. As a result, back EMFs of the motor tend to be significantly nonsinusoidal [9]. For this kind of back EMF, the iron loss modeled in SRF1 will mismatch with a physical view that is explained later in this article, then leading to a loss minimization error. Some other model-based strategies [10], [11] utilized a Steinmetz equation to represent the iron loss, but the mismatch is suffered as well.

The CLM strategy aims to produce a desired electromagnetic torque with minimal copper loss [12]–[14]. By keeping constant the dot product of current vector and back EMF vector, the torque can be produced free of ripple. Meanwhile, winding copper loss can be minimized by aligning the two vectors, so as to enhance the motor efficiency. This strategy is applicable for PMSM with nonsinusoidal back EMF (NS-PMSM). However, it cannot drive the motor to true minimal-loss (ML) points because the stator iron loss, which is also affected by the current vector, is out of consideration. Therefore, the CLM is actually a pseudoloss-minimization strategy. In addition, the iron loss torque cannot

Manuscript received May 10, 2019; revised August 8, 2019, September 26, 2019, and October 29, 2019; accepted December 12, 2019. Date of publication December 22, 2019; date of current version April 22, 2020. Recommended for publication by Associate Editor A. K. Gupta. *(Corresponding author: Haitao Zhang.)*

The authors are with the School of Automation, Northwestern Polytechnical University, Xi'an 710072, China (e-mail: zhanghaitao@mail.nwpu.edu.cn; doumf@nwpu.edu.cn; 805100759@mail.nwpu.edu.cn).

Color versions of one or more of the figures in this article are available online at http://ieeexplore.ieee.org.

Digital Object Identifier 10.1109/TPEL.2019.2961689

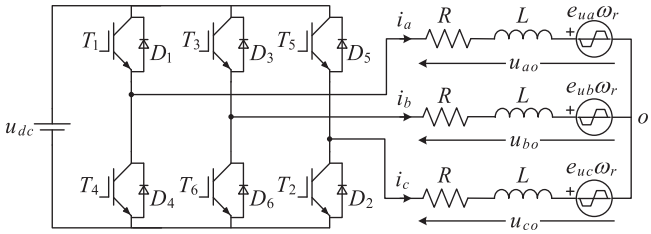

Fig. 1. Circuital scheme of a NS-PMSM drive.

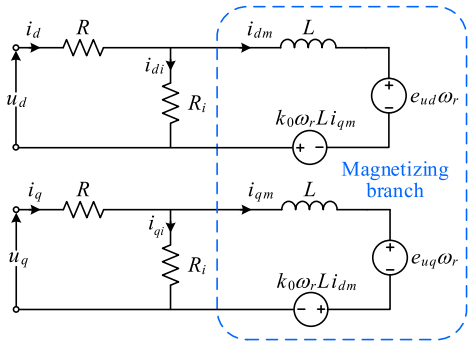

Fig. 2. Equivalent d- and q-axis circuits of a NS-PMSM in SRF1 with stator iron loss included.

be compensated, leading to an error in generating the desired torque [15].

In [16] and [17], the optimal current solution was determined based on a FE iron loss model, so as to cover the case of nonsinusoidal back EMFs and current. A main challenge of this strategy is that large amounts of efforts have to be devoted to FE simulations under various operating conditions. A lookup table is also required to store the current solutions for real-time implementation, resulting in a bulky firmware.

In [18] and [19], multiple synchronous reference frames (MSRF) theory was introduced to address harmonic issues of permanent-magnet (PM) motor. However, this theory is not applicable for loss minimization of NS-PMSM because the stator iron loss cannot be evaluated. This article combines the theories of MSRF and iron loss resistance to develop a new model of NS-PMSM, based on which the stator iron loss can be evaluated precisely and matches well with the physical view. Then, the total stator loss, consisting of copper loss and iron loss, is minimized subjecting to constraints of ripple-free torque and finite dc supply voltage. The optimal current is determined with a simple expression, which can be implemented effortlessly. A comparison with CLM strategy indicates that the proposed strategy performs better in reducing the stator loss and enhancing the motor efficiency especially in high-speed region of the motor. Compared to traditional model-based strategy, a more precise loss-minimal-point tracking is realized. Finally, performances of the proposed strategy are validated experimentally on a 3.8-kW NS-PMSM setup which is designed to drive a fuel pump in aerospace.

II. Model of NS-PMSM With Stator Iron Loss

A. Mismatch Between Iron Loss in SRF1 and Physical View

Considering a NS-PMSM drive with three-phase windings, the circuital scheme is shown in Fig. 1. The windings are represented by the phase resistance R, inductance L, and back EMFs $e_{uj}\,\omega_r\,(j = a, b, c)$, where ω_r is the rotor speed, and e_{uj} are the ratios of back EMFs to ω_r. Phase voltages u_{jo} are measured with respect to the neutral point of the windings, denoted with o. $u_{\rm dc}$ is the dc supply voltage. Phase currents i_j are positive when entering into the motor. With reference to Fig. 1, the phase voltage equation in *ABC* frame can be expressed as

$$\begin{bmatrix} u_{ao} \\ u_{bo} \\ u_{co} \end{bmatrix} = R \begin{bmatrix} i_a \\ i_b \\ i_c \end{bmatrix} + Lp \begin{bmatrix} i_a \\ i_b \\ i_c \end{bmatrix} + \omega_r \begin{bmatrix} e_{\rm ua} \\ e_{ub} \\ e_{uc} \end{bmatrix} \tag{1}$$

where the symbol "p" represents a differential operation.

The equation that transforms variables from *ABC* frame to SRF1 with invariant power is generally known as

$$\mathrm{T}_{\mathrm{ABC-SRF1}} = \sqrt{\frac{2}{3}} \begin{bmatrix} \cos\theta_e & \cos\left(\theta_e - \frac{2\pi}{3}\right) & \cos\left(\theta_e + \frac{2\pi}{3}\right) \\ -\sin\theta_e & -\sin\left(\theta_e - \frac{2\pi}{3}\right) & -\sin\left(\theta_e + \frac{2\pi}{3}\right) \end{bmatrix} \tag{2}$$

where θ_e is the rotor electrical position. Applying (2) to (1) yields

$$\begin{bmatrix} u_d \\ u_q \end{bmatrix} = (R + Lp) \begin{bmatrix} i_d \\ i_q \end{bmatrix} + k_0\omega_r L \begin{bmatrix} -i_q \\ i_d \end{bmatrix} + \omega_r \begin{bmatrix} e_{ud} \\ e_{uq} \end{bmatrix} \tag{3}$$

where the subscripts d and q represent the direct axis and quadrature axis of SRF1, and k_0 is the number of rotor pole pairs. Based on (3), the equivalent d- and q-axis circuits of a NS-PMSM are described in Fig. 2. The resistance R_i is inserted to represent the stator iron loss. According to Fig. 2, the current equation is written as

$$\begin{cases} L\omega_r \frac{di_{dm}}{d\theta_e} - k_0\omega_r L i_{qm} - R_i i_{di} = -e_{ud}\omega_r \\ L\omega_r \frac{di_{qm}}{d\theta_e} + k_0\omega_r L i_{dm} - R_i i_{qi} = -e_{uq}\omega_r \\ i_d = i_{dm} + i_{di} \\ i_q = i_{qm} + i_{qi}. \end{cases} \tag{4}$$

To explain the mismatch between the iron loss in SRF1 and the physical view, a 3.8-kW NS-PMSM is taken as a general example. Rated data of the motor are specified in the Appendix. Due to the radial magnetization and concentrated winding applied, back EMF of the motor includes significant fifth and seventh harmonics. As a result, the measured e_{ud} and e_{uq} pulsate in a period of $\pi/3$ electrical radian, as Fig. 3 shows. Now, consider a no-load operation of the motor at rated speed ω_N. Substituting $i_d = i_q = 0$ into (4), the currents i_{di} and i_{qi} can be solved. Then, the stator iron loss $P_{ir,\mathrm{SRF1}}$ is calculated through

$$P_{ir,\mathrm{SRF1}} = R_i \left(i_{di}^2 + i_{qi}^2\right) \tag{5}$$

and plotted in Fig. 3. It is shown that the loss pulsates in the period of $\pi/3$ electrical radian as well.

The physical view has been widely accepted that dynamic iron loss depends on distributions of flux density B and time derivative dB/dt in the stator core [20], [21]. In no-load operation

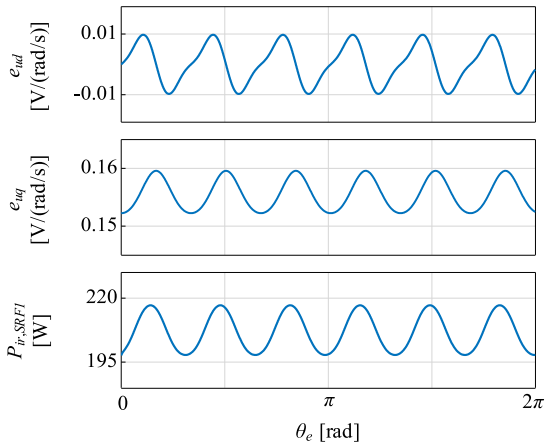

Fig. 3. Measured e_{ud} and e_{uq} of the 3.8-kW motor and the no-load stator iron loss evaluated in SRF1.

of the motor, armature field can be ignored. If we view from SRF1 and neglect a slotted effect, the distributions of *B* and d*B*/d*t* will be constant regardless of the rotor position, resulting in a constant stator iron loss as well. Obviously, pulsated $P_{ir,\mathrm{SRF1}}$ mismatches with the physical view.

Traditional model-based strategy in SRF1 can be described by an optimizing problem as [8]

$$\text{Minimize } P_{s,\mathrm{SRF1}} = P_{ir,\mathrm{SRF1}} + R\left(i_d^2 + i_q^2\right) \tag{6}$$

subjecting to the torque constraint

$$i_{dm}e_{ud} + i_{qm}e_{uq} = T_{e,\mathrm{cmd}}.$$

$P_{s,\mathrm{SRF1}}$ represents the total stator loss in SRF1. $T_{e,\mathrm{cmd}}$ is the load command. When solving the optimal solution of $i_{d,q,}$ two disadvantages are suffered, one of which is that the mismatch between $P_{ir,\mathrm{SRF1}}$ and the physical view may cause an error to the optimal $i_{d,q}$. As a result, minimized stator loss will not be achieved. This disadvantage has been validated experimentally later in this article. The other one is that since e_{ud} and e_{uq} contain ac components, currents i_{dm} and i_{qm} also contain ac components to produce a constant torque, so the differential items $di_{dm}/d\theta_e$ and $di_{qm}/d\theta_e$ in (4) cannot be ignored. Then, i_{dm}, i_{qm} and i_{di}, i_{qi} are difficult to be expressed in closed forms with $i_{d,q,}$ which brings trouble to solve the optimal $i_{d,q}$ analytically.

B. New Model of NS-PMSM With Stator Iron Loss

The MSRF theory [18], [19] indicates that an *n*th harmonic component in *ABC* frame can be transformed to a constant variable in a rotary frame with a synchronous speed of $nk_0\omega_r$. Here, the rotary frame is denoted as SRF*n* for short. With the first, fifth, and seventh harmonics examined, the phase current i_a and EMF ratio e_{ua} can be expressed as

$$i_a = \sum_n I_n \sin(n\theta_e + \theta_n) \qquad n = 1, 5, 7 \tag{7}$$

$$e_{ua} = \sum_n E_n \sin(n\theta_e) \qquad n = 1, 5, 7 \tag{8}$$

where I_n and E_n are the *n*th harmonic magnitudes. θ_n represents the offset angle between the *n*th harmonics of i_a and e_{ua}. The expressions for Phases *B* and *C* can be obtained by displacing θ_e with $(\theta_e - 2\pi/3)$ and $(\theta_e - 4\pi/3)$, respectively. Referring to (7) and (8), (1) can be decomposed to three harmonic voltage equations as (9), shown at the bottom of this page, where

$$u_{jo} = \sum_n u_{jn}, \qquad n = 1, 5, 7 \text{ and } j = a, b, c.$$

The equations that transform variables from *ABC* frame to SRF5 and SRF7 are written as [19]

$$T_{\mathrm{ABC-SRF5}} = \sqrt{\frac{2}{3}}\begin{bmatrix} \cos 5\theta_e & \cos\left(5\theta_e + \frac{2\pi}{3}\right) & \cos\left(5\theta_e - \frac{2\pi}{3}\right) \\ -\sin 5\theta_e & -\sin\left(5\theta_e + \frac{2\pi}{3}\right) & -\sin\left(5\theta_e - \frac{2\pi}{3}\right) \end{bmatrix} \tag{10}$$

$$T_{\mathrm{ABC-SRF7}} = \sqrt{\frac{2}{3}}\begin{bmatrix} \cos 7\theta_e & \cos\left(7\theta_e - \frac{2\pi}{3}\right) & \cos\left(7\theta_e + \frac{2\pi}{3}\right) \\ -\sin 7\theta_e & -\sin\left(7\theta_e - \frac{2\pi}{3}\right) & -\sin\left(7\theta_e + \frac{2\pi}{3}\right) \end{bmatrix}. \tag{11}$$

Applying $T_{\mathrm{ABC\text{-}SRF1}}$, $T_{\mathrm{ABC\text{-}SRF5}}$, and $T_{\mathrm{ABC\text{-}SRF7}}$ to (9) shown at the bottom of this page, at the respective cases of $n = 1$, $n = 5$, and $n = 7$, the model of NS-PMSM is yielded in MSRF as

$$\begin{bmatrix} u_{\mathrm{d}}^n \\ u_q^n \end{bmatrix} = R\begin{bmatrix} i_d^n \\ i_q^n \end{bmatrix} + nk_0\omega_r L\begin{bmatrix} -i_q^n \\ i_d^n \end{bmatrix} + \omega_r \begin{bmatrix} 0 \\ e_q^n \end{bmatrix}, n = 1, 5, 7 \tag{12}$$

where

$$i_d^n = \sqrt{\frac{3}{2}} I_n \sin\theta_n,\ i_q^n = -\sqrt{\frac{3}{2}} I_n \cos\theta_n \text{ and } e_q^n = -\sqrt{\frac{3}{2}} E_n.$$

The superscript *n* indicates the variable adhered in SRF*n*. The spatial relationship between different frames is shown in Fig. 4. According to the iron loss resistance theory [5], stator iron loss caused by the *n*th harmonic airgap field, denoted as P_{ir}^n, can be represented by a virtual resistance R_i^n in parallel with magnetizing branches of d^n- and q^n- axis circuits. With reference to (12), a new model of NS-PMSM considering the iron loss is described in Fig. 5. Then, current equation is written

$$\begin{bmatrix} u_{an} \\ u_{bn} \\ u_{cn} \end{bmatrix} = RI_n \begin{bmatrix} \sin(n\theta_e + \theta_n) \\ \sin\left(n\theta_e - \frac{2\pi n}{3} + \theta_n\right) \\ \sin\left(n\theta_e - \frac{4\pi n}{3} + \theta_n\right) \end{bmatrix} + Lk_0\omega_r nI_n \begin{bmatrix} \cos(n\theta_e + \theta_n) \\ \cos\left(n\theta_e - \frac{2\pi n}{3} + \theta_n\right) \\ \cos\left(n\theta_e - \frac{4\pi n}{3} + \theta_n\right) \end{bmatrix} + \omega_r E_n \begin{bmatrix} \sin(n\theta_e) \\ \sin\left(n\theta_e - \frac{2\pi n}{3}\right) \\ \sin\left(n\theta_e - \frac{4\pi n}{3}\right) \end{bmatrix}, n = 1, 5, 7 \tag{9}$$

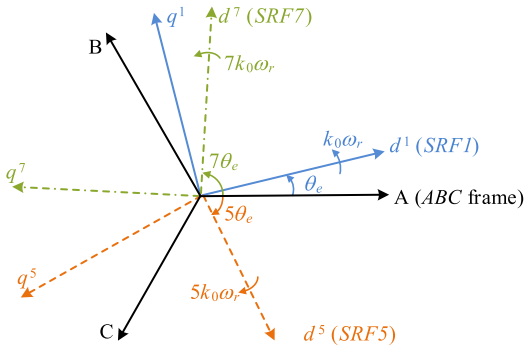

Fig. 4. Spatial relationship between different frames.

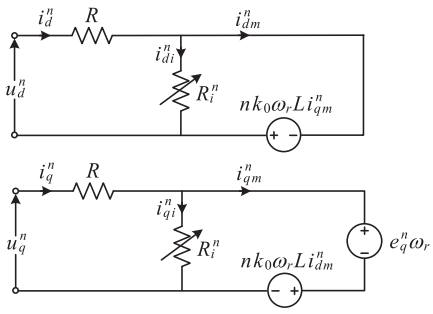

Fig. 5. New model of NS-PMSM in SRFn with stator iron loss included.

as

$$\begin{cases} i_{di}^n + i_{dm}^n = i_d^n \\ i_{qi}^n + i_{qm}^n = i_q^n \\ i_{di}^n = -k_1^n i_{qm}^n \\ i_{qi}^n = k_1^n i_{dm}^n + k_2^n \end{cases} \tag{13}$$

where

$$k_1^n = \frac{nk_0\omega_r L}{R_i^n} \text{ and } k_2^n = \frac{\omega_r e_q^n}{R_i^n}.$$

Eliminating i_{di}^n and i_{qi}^n yields

$$\begin{bmatrix} i_{\mathrm{dm}}^n \\ i_{qm}^n \end{bmatrix} = \begin{bmatrix} 1 & -k_1^n \\ k_1^n & 1 \end{bmatrix}^{-1} \begin{bmatrix} i_d^n \\ i_q^n - k_2^n \end{bmatrix}. \tag{14}$$

Then P_{ir}^n is derived as

$$\begin{aligned} P_{\mathrm{ir}}^n &= R_i^n \left(i_{di}^{n2} + i_{qi}^{n2}\right) = R_i^n \left[\left(\mathrm{k}_1^n i_{qm}^n\right)^2 + \left(k_1^n i_{dm}^n + k_2^n\right)^2\right] \\ &= \frac{R_i^n \left[\left(\mathrm{k}_1^n i_q^n\right)^2 + \left(k_1^n i_d^n + k_2^n\right)^2\right]}{1 + k_1^{n2}}. \end{aligned} \tag{15}$$

In general, the total stator iron loss $P_{ir,\mathrm{MSRF}}$ can be equivalent to a sum of the partial iron losses caused by the harmonic fields [16], [22], that is

$$P_{ir,\mathrm{MSRF}} = \sum_n P_{ir}^n. \tag{16}$$

Now, consider the no-load operation of the motor. Substituting $i_d^n = i_q^n = 0$ into (15) and (16), the stator iron loss is obtained as

$$P_{ir,\mathrm{MSRF}} = \sum_{n=1,5,7} \frac{R_i^n k_2^{n2}}{1 + k_1^{n2}} \tag{17}$$

which is a constant regardless of the rotor position and matches well with the physical view. Moreover, since i_{dm}^n and i_{qm}^n are constant in stable operation of the motor, there is no differential item included in (13). Then, i_{dm}^n, i_{qm}^n and i_{di}^n, i_{qi}^n can be expressed in closed forms with $i_{d,q}^n$, which brings convenience to solve the optimal $i_{d,q}^n$ analytically.

Experimental study in [23] indicates that the iron loss resistance has a linear relationship with synchronous angular velocity of the rotary airgap field. Therefore, R_i^n can be expressed as $(ank_0\omega_r + b)$. In order to determine the coefficients a and b, a no-load test of the motor should be carried out to measure the active input power under various speeds. Since the copper loss is very small, the input power can be approximated as the stator iron loss. In the test, six-step mode of the inverter is preferred because it is simple to be implemented and the output voltages are without pulsewidth modulation (PWM) carrier harmonics. By substituting R_i^n into (17) and then fitting $P_{ir,\mathrm{MSRF}}$ to the measured iron loss, a and b can be obtained.

III. Proposed Loss-Minimization Strategy

A. Proposed Strategy

According to the circuits in Fig. 5, the electromagnetic torque T_e can be written as

$$T_e = T_0 + T_{\mathrm{ripple}} \tag{18}$$

where T_0 is a constant torque produced by interactions between i_{qm} and e_q in the same frame, and the ripple torque

$$\begin{aligned} T_{\mathrm{ripple}} = T_{6d}\sin 6\theta_e + T_{6q}\cos 6\theta_e + T_{12d}\sin 12\theta_e \\ + T_{12q}\cos 12\theta_e \end{aligned}$$

is produced by interactions between i_{qm} and e_q in different frames. $T_0, T_{6d}, T_{6q}, T_{12d}$, and T_{12q} can be expressed in a matrix form as

$$\begin{bmatrix} T_0 \\ T_{6d} \\ T_{6q} \\ T_{12d} \\ T_{12q} \end{bmatrix} = \underbrace{\begin{bmatrix} 0 & e_q^1 & 0 & e_q^5 & 0 & e_q^7 \\ -e_q^5 - e_q^7 & 0 & -e_q^1 & 0 & e_q^1 & 0 \\ 0 & e_q^7 - e_q^5 & 0 & -e_q^1 & 0 & e_q^1 \\ 0 & 0 & -e_q^7 & 0 & -e_q^5 & 0 \\ 0 & 0 & 0 & -e_q^7 & 0 & -e_q^5 \end{bmatrix}}_{\boldsymbol{E_m}} \underbrace{\begin{bmatrix} i_{dm}^1 \\ i_{qm}^1 \\ i_{dm}^5 \\ i_{qm}^5 \\ i_{dm}^7 \\ i_{qm}^7 \end{bmatrix}}_{\boldsymbol{I_m}}. \tag{19}$$

Rewriting (14) as

$$\begin{bmatrix} i_d^n \\ i_q^n \end{bmatrix} = \begin{bmatrix} 1 & -k_1^n \\ k_1^n & 1 \end{bmatrix} \begin{bmatrix} i_{\mathrm{dm}}^n \\ i_{qm}^n \end{bmatrix} + \begin{bmatrix} 0 \\ k_2^n \end{bmatrix} \tag{20}$$

the winding copper loss P_{cu} can be derived as

$$\begin{aligned} P_{\mathrm{cu}} &= R\sum_{\mathrm{n}=1,5,7}\left(i_d^{n2}+i_q^{n2}\right) \\ &= R\sum_{n=1,5,7}\left[\left(i_{dm}^n-k_1^n i_{qm}^n\right)^2+\left(k_1^n i_{dm}^n+k_2^n+i_{qm}^n\right)^2\right]. \end{aligned} \tag{21}$$

Based on (15), (16), and (21), the total stator loss P_s can be expressed in a quadric form as

$$P_s = P_{ir,\mathrm{MSRF}} + P_{cu} = \frac{1}{2}\boldsymbol{I_m^T Q I_m} + \boldsymbol{h I_m} + c \tag{22}$$

where

$$\begin{cases} \boldsymbol{Q} = \mathrm{diag}\left(Q^1, Q^1, Q^5, Q^5, Q^7, Q^7\right) \\ \boldsymbol{h} = \left[h_d^1, h_q^1, h_d^5, h_q^5, h_d^7, h_q^7\right] \\ c = \sum\limits_{n=1,5,7}\left(R+R_{\mathrm{i}}^n\right)k_2^{n2} \\ Q^n = 2\left(R+k_1^{n2}R+k_1^{n2}R_{\mathrm{i}}^n\right) \\ h_d^n = 2k_1^n k_2^n\left(R+R_i^n\right) \\ h_q^n = 2Rk_2^n. \end{cases} \tag{23}$$

In order to minimize the total stator loss and simultaneously suppress the ripple torque, an optimizing problem is developed as

$$\text{Minimize } P_s$$

subjecting to the constraints

$$\begin{cases} T_0 = T_{e,\mathrm{cmd}} & \text{(24a)} \\ T_{6d} = T_{6q} = T_{12d} = T_{12q} = 0 & \text{(24b)} \\ u_p \le u_{\mathrm{dc}} & \text{(24c)} \end{cases}$$

where u_p is peak value of the motor line voltage. Without considering the constraint (24c), solution to the problem can be solved by Lagrange multiplier method as

$$\begin{bmatrix} \boldsymbol{I_m} \\ \boldsymbol{\lambda} \end{bmatrix} = \begin{bmatrix} \boldsymbol{Q} & \boldsymbol{E_m^T} \\ \boldsymbol{E_m} & \boldsymbol{0} \end{bmatrix}^{-1} \begin{bmatrix} -\boldsymbol{h}^{\mathrm{T}} \\ \boldsymbol{z} \end{bmatrix} \tag{25}$$

where $\boldsymbol{z} = [T_{e,\mathrm{cmd}}, 0, 0, 0, 0]^T$, and $\boldsymbol{\lambda}$ is the Lagrange multiplier vector. Expanding (25) and substituting the resulted i_{dm}^n and i_{qm}^n into (20), optimal currents $i_{d,\mathrm{opt}}^n$ and $i_{q,\mathrm{opt}}^n$ can be derived as

$$\begin{cases} i_{d,\mathrm{opt}}^n \approx i_{dm}^n = \mathrm{sign}(n)k_3^n & \text{(26a)} \\ i_{q,\mathrm{opt}}^n \approx i_{qm}^n + k_2^n = k_4^n T_{e,\mathrm{cmd}} + k_2^n & \text{(26b)} \end{cases}$$

where

$$\begin{cases} \mathrm{sign}(n) = \begin{cases} -1 & n=1,7 \\ 1 & n=5 \end{cases} \\ k_3^n = e_q^n \frac{e_q^1 h_d^1 - e_q^5 h_d^5 + e_q^7 h_d^7}{Q^1(e_q^1)^2 + Q^5(e_q^5)^2 + Q^7(e_q^7)^2} \\ k_4^n = \begin{cases} k_5 e_q^1\left(e_q^5+e_q^7\right) & n=1 \\ k_5 e_q^5\left(e_q^7-e_q^5\right) & n=5 \\ k_5 e_q^7\left(e_q^5-e_q^7\right) & n=7 \end{cases} \\ k_5 = \frac{1}{\left((e_q^1)^2-(e_q^5-e_q^7)^2\right)(e_q^5+e_q^7)}. \end{cases} \tag{27}$$

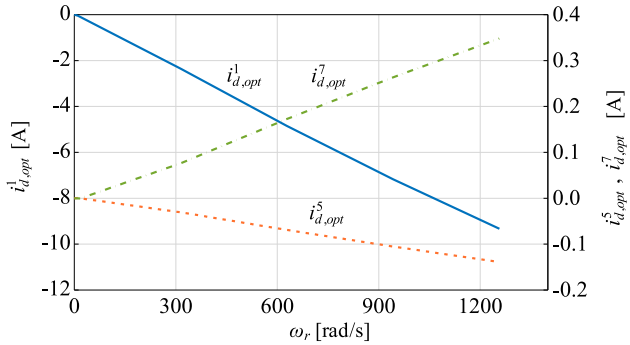

Fig. 6. Behaviors of $i_{d,\mathrm{opt}}^n$ versus rotor speed calculated from the 3.8-kW motor.

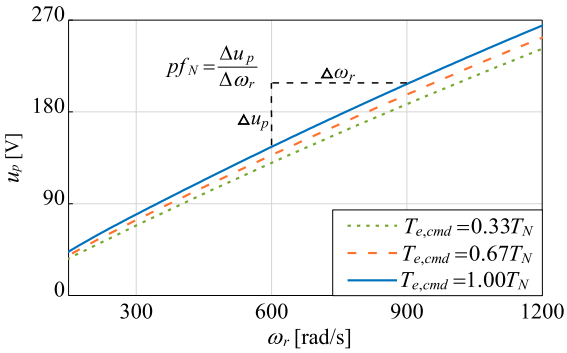

Fig. 7. Behavior of u_p versus rotor speed under different $T_{e,\mathrm{cmd}}$.

In the derivation, k_1^n in (20) is approximated as zero because L is usually far less than a. For a manufactured NS-PMSM, e_q^n are constant, and then $i_{d,\mathrm{opt}}^n$ only depends on the rotor speed. Fig. 6 shows the behaviors of $i_{d,\mathrm{opt}}^n$ calculated from the 3.8-kW motor. It is seen that $i_{d,\mathrm{opt}}^n$ are almost proportional to the rotor speed.

Equation (26b) indicates that $i_{q,\mathrm{opt}}^n$ have linear relationships with $T_{e,\mathrm{cmd}}$. The slopes k_4^n only depend on e_q^n. The item k_2^n in (26b) acts to compensate for the iron loss toque. The optimal currents of (26) are simple in expression and can be implemented online under various speed and load conditions. Then, amounts of efforts and lookup table are not necessary.

The motor is driven by the proposed strategy. Under different $T_{e,\mathrm{cmd}}$, behaviors of u_p versus rotor speed ω_r are plotted in Fig. 7. It is seen that u_p is almost proportional to ω_r, and gets greater with $T_{e,\mathrm{cmd}}$ increasing. Specially, the proportional factor under rated load is denoted as pf_N. Now, consider a certain operation. If u_{dc} is greater than the corresponding u_p, the motor can be operated in two modes, as shown in Fig. 8. In the torque control mode, $T_{e,\mathrm{cmd}}$ is determined directly by the system desired torque $T_{e,\mathrm{des}}$. In the speed control mode, $T_{e,\mathrm{cmd}}$ is determined by the output of a speed controller. Reference of the controller is the system desired speed $\omega_{r,\mathrm{des}}$. If u_{dc} is less than the corresponding u_p, the operation cannot be maintained anymore, which may result in a greater stator loss and significant torque ripple. In order to suppress the stator loss and torque ripple, the motor has to be operated in the speed control mode

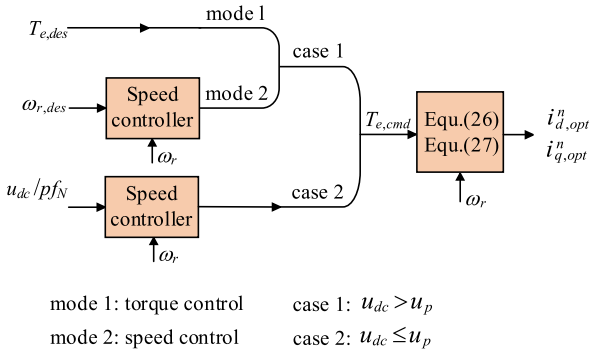

Fig. 8. Proposed strategy considering lower dc supply voltage.

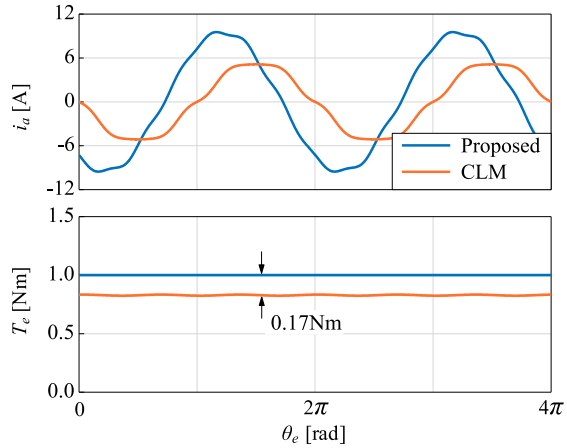

Fig. 9. Instantaneous phase-A currents and electromagnetic torques of the proposed and CLM strategies under the conditions $T_{e,\mathrm{cmd}} = 1.0$ N·m and $\omega_r = \omega_N$.

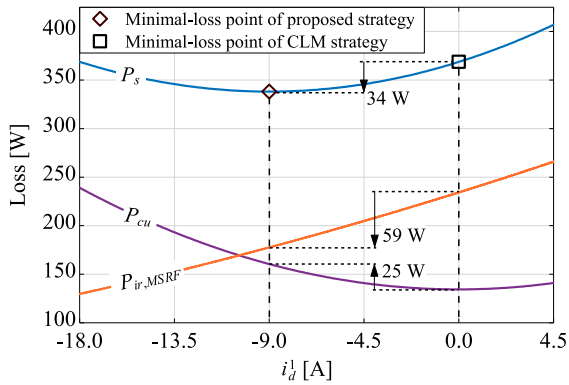

Fig. 10. Behaviors of the iron loss $P_{ir,\mathrm{MSRF}}$, copper loss P_{cu}, and total stator loss P_s versus i^1_d under the rated load and speed.

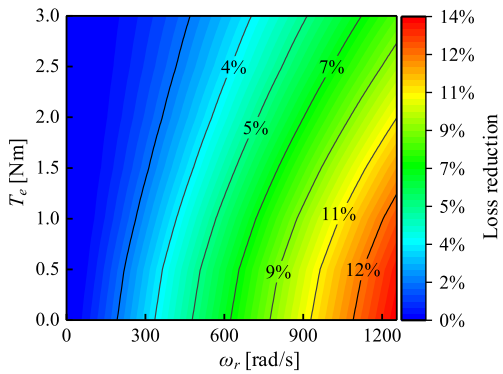

Fig. 11. Loss reduction map of various loads and speeds.

with a lower reference. As Fig. 8 shows, the reference is given as the ratio of u_{dc} to pf_N. In this case, $T_{e,\mathrm{cmd}}$ is determined by output of the speed controller to match the load adaptively.

B. Comparison With CLM Strategy

The CLM strategy in MSRF can be described by an optimizing problem as

$$\mathrm{Minimize} R\boldsymbol{I}_{\boldsymbol{m}}^{\boldsymbol{T}}\boldsymbol{I}_{\boldsymbol{m}}$$

subjecting to the constraint $\boldsymbol{E_m}\,\boldsymbol{I_m} = \boldsymbol{z}$. Solving the problem by the Lagrange multiplier method, the CLM current vector $\boldsymbol{I}_{\mathbf{CLM}}$ is obtained as

$$\boldsymbol{I}_{\mathbf{CLM}} = \left(\begin{bmatrix} \mathbf{[1]} & \boldsymbol{E}_{\boldsymbol{m}}^{T} \\ \boldsymbol{E_m} & \mathbf{0} \end{bmatrix}^{-1} \begin{bmatrix} \mathbf{0} \\ \boldsymbol{z} \end{bmatrix} \right)_6$$

$$= T_{e,\mathrm{cmd}} \left[0, k_4^1, 0, k_4^5, 0, k_4^7\right]^T$$

where **[1]** is an identity matrix of six orders, and the subscript "6" represents the first six rows of the matrix. Since there are no d-axis currents included in $\boldsymbol{I}_{\mathbf{CLM}}$, the corresponding phase current appears a phase lag and less amplitude compared to current of the proposed strategy, as shown in Fig. 9. The figure also shows a torque error of 0.17 N·m for the CLM strategy because the iron loss torque is not compensated. By comparison, precise electromagnetic torque is produced by the proposed strategy. If we substitute $\omega_r = 0$ into (26), it is interesting to find that the vector $[i^1_{d,\mathrm{opt}}, i^1_{q,\mathrm{opt}}, i^5_{d,\mathrm{opt}}, i^5_{q,\mathrm{opt}}, i^7_{d,\mathrm{opt}}, i^7_{q,\mathrm{opt}}]^T$ equals to $\boldsymbol{I}_{\mathbf{CLM}}$, that means the CLM strategy is actually a special case of the proposed strategy that ω_r equals to zero.

For a given i^1_d, other i^n_d and i^n_d can be determined under the constraints of (24a) and (24b). Then, the iron loss $P_{ir,\mathrm{MSRF}}$, copper loss P_{cu}, and total stator loss P_s can be calculated through the equations of (16), (21), and (22). Fig. 10 shows behaviors of the losses versus i^1_d under the rated load and speed. It is seen that the CLM strategy indeed produces the least copper loss at the i^1_d of 0, but the stator loss is not minimized because a greater iron loss is caused. The proposed strategy, although causes an increase of 25-W copper loss, can reduce more iron loss of 59 W at the i^1_d of -9 A. As a result, the total stator loss is reduced by 34 W and reaches the real minimal value.

A variable defined as $(1 - P_{s,\mathrm{opt}}/P_{s,\mathrm{CLM}})$ is used to evaluate the loss reductions between the two strategies. $P_{s,\mathrm{opt}}$ and $P_{s,\mathrm{CLM}}$ represent the stator losses of the proposed and CLM strategies, respectively. Fig. 11 shows the loss reduction map of various load and speed conditions. It seems that the proposed strategy performs better when the motor operates in a high-speed and light-load region, where the loss reduction comes to as great as 12%. With the load increasing, the reduction gets less

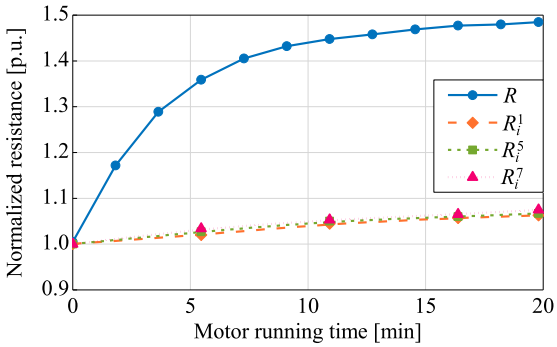

Fig. 12. Measured phase resistance R and iron loss resistances R_i^n under rated operation of the motor.

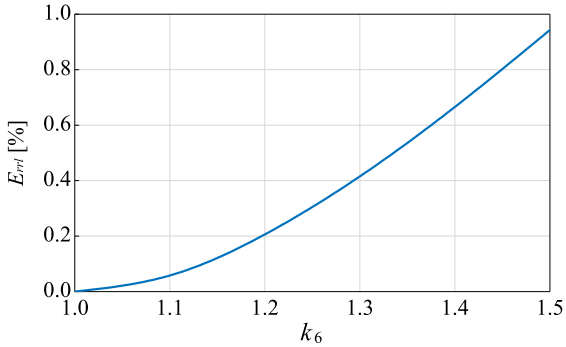

Fig. 13. Behavior of E_{rrl} versus k_6 under rated operation of the motor.

slightly, reaching about 9% at the rated load. With the rotor speed decreasing, the reduction gets to zero rapidly.

C. Robustness to Motor Parameters

It is noted from (27) that the optimal currents $i_{d,\mathrm{opt}}^n$ and $i_{q,\mathrm{opt}}^n$ depend on the motor parameters of phase resistance R, iron loss resistance R_i^n, inductance L, and EMF ratios e_q^n. For a NS-PMSM with surface-mounted structure, the equivalent (augmented) airgap prevents the stator core from saturation, so the inductance L does not change a lot during motor operation. In aerospace application with a high-reliability requirement, SmCo magnet is generally used due to its steady magnetic performance under field-weakening and harsh temperature conditions, so e_q^n are almost constant in operation. To confirm the behaviors of R and R_i^n, their value curves are tested under rated operation of the 3.8-kW motor. At beginning of the test, winding and stator core temperatures equal to the ambient temperature of 25 °C. Values of R and R_i^n under this condition are denoted as respective R_a and R_{ia}^n. With the motor running, test results of R and R_i^n are shown in Fig. 12, which is normalized to R_a and R_{ia}^n. It is seen that, both of R and R_i^n get greater because the winding and stator core are heated by the loss power. About 20 min later, the motor comes to a heat equilibrium. R_i^n only increases by 7% during the operation, while R increases by as large as 50%, which may result in inaccuracies of the proposed strategy.

Assume that in a certain operation, R increases from R_a to $k_6 R_a$, other parameters of L, e_q^n and R_i^n remain unchanged. Then, the total stator loss, alternatively denoted as P_{sn}, is obtained as

$$P_{sn} = P_s|_{R=k_6 R_a} \tag{28}$$

where P_s is expressed as (22). To evaluate the effect of R variation on accuracy of the proposed strategy, a variable of loss control error E_{rrl} is introduced as

$$E_{rrl} = \frac{\hat{P}_{sn,\mathrm{opt}}}{P_{sn,\mathrm{opt}}} - 1$$

where $P_{sn,\mathrm{opt}}$ is the optimal stator loss considering R variation. It is calculated by substituting $R = k_6 R_a$ into (26) and (27), then substituting the resulted $i_{d,\mathrm{opt}}^n$ and $i_{q,\mathrm{opt}}^n$ into (28). $\hat{P}_{sn,\mathrm{opt}}$ is the optimal stator loss without considering R variation. It is calculated by substituting $R = R_a$ into (26) and (27), then substituting the resulted $i_{d,\mathrm{opt}}^n$ and $i_{q,\mathrm{opt}}^n$ into (28). At the rated operation, the behavior of E_{rrl} versus k_6 is calculated and shown in Fig. 13. It is seen that E_{rrl} increases with k_6 becoming greater. Given k_6 as 1.5, E_{rrl} under various operations is shown in Fig. 14, which indicates that E_{rrl} increases when the motor operates in a higher speed with lower load. The greatest value of E_{rrl} appears in a very small level of 1.9%, that means the proposed strategy has a good robustness to the variation of winding phase resistance.

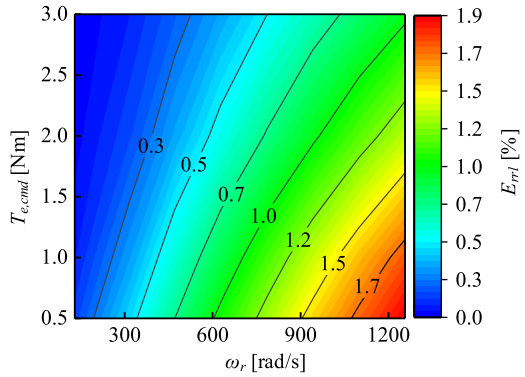

Fig. 14. E_{rrl} under various operations of the motor when k_6 equals to 1.5.

IV. Experiment

A. Experimental Setup

Fig. 15 shows the experimental setup of the 3.8-kW NS-PMSM. It is designed to work at a 15-km high altitude for fuel pump driving. The stator core is designed to be cooled by oil, but in the lab experiments, water is used instead of oil for safety concern. A high-speed dynamometer is coupled with the motor to apply a load torque which is controlled proportionally to the rotor speed. The device DSP6001 is used to adjust the load proportional coefficient, so that the motor can be operated stably under various loads and speeds. The device also acts to measure the axis torque of the motor, which is approximated as the electromagnetic torque T_e. A resolver is mounted to measure the rotor position. A power module PM75DSA120 is utilized as

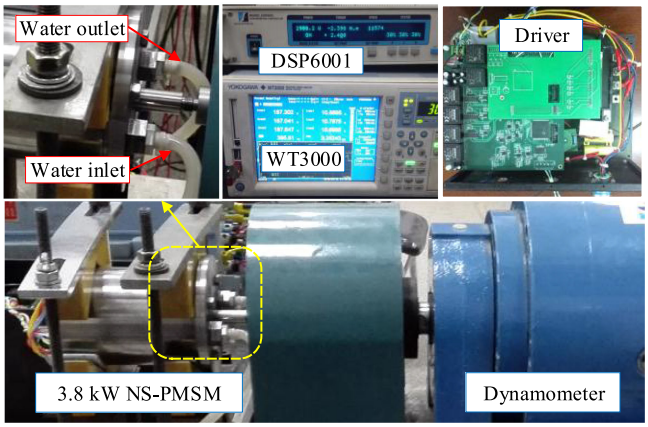

Fig. 15. Experimental setup of the 3.8-kW NS-PMSM.

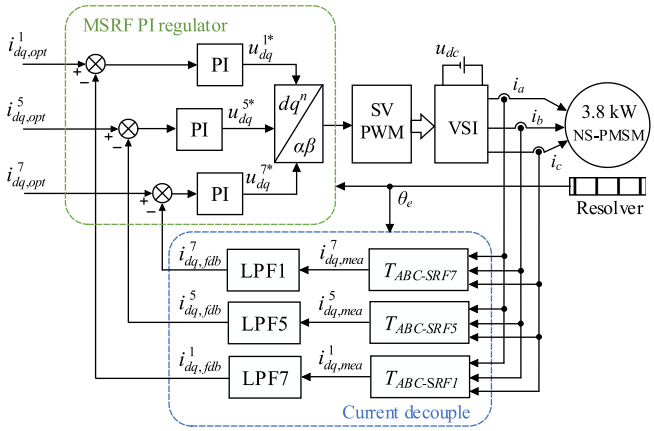

Fig. 16. Current control loop scheme.

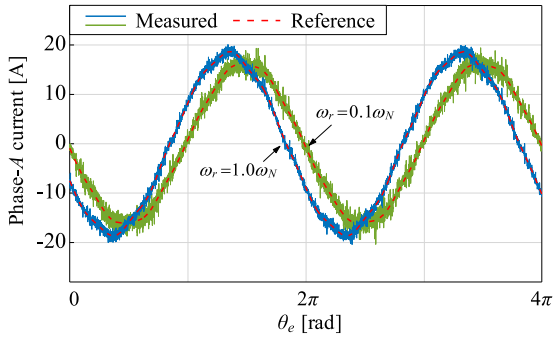

Fig. 17. Measured instantaneous phase-*A* currents under a low speed of $0.1\omega_N$ and a high speed of $1.0\omega_N$. $T_{e,\mathrm{cmd}}$ is given as T_N.

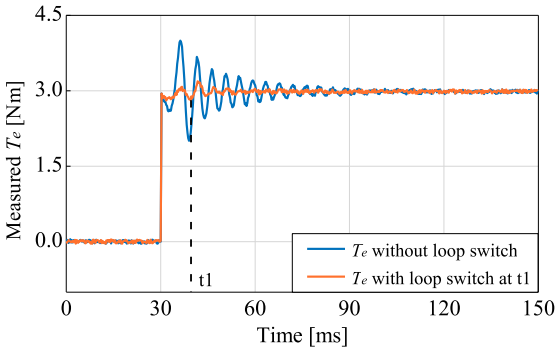

Fig. 18. Measured torque transient response under a step of $T_{e,\mathrm{cmd}}$ from 0 to T_N.

the voltage source inverter (VSI). The phase current, losses, and motor efficiency are tested by the power analyzer WT3000.

Fig. 16 shows a scheme of the current control loop. The current decouple module transforms measured three-phase currents to the d^n- and q^n- axis variables $i^n_{dq,\mathrm{mea}}$. Then, low-pass Butterworth filters LPF*n* are applied to extract constant feedback currents $i^n_{dq,fdb}$. After PI regulations in MSRF, the resulted voltage commands u^n_{dq} are synthesized in the stationary α-β frame, and then fed to the space vector pulsewidth modulation (SVPWM) generating module. With this control scheme, the fifth and seventh current harmonic references can be well tracked without the limitation of current-loop bandwidth. Moreover, voltage disturbances from the VSI dead-time effect and the back EMF harmonics can be compensated adaptively by the PI regulators. Both the proposed strategy and control scheme are implemented on a DSP platform of TMS320F28335. The data of $i^n_{dq,\mathrm{opt}}$, $i^n_{dq,\mathrm{mea}}$, and $i^n_{dq,fdb}$ are transferred from DSP to PC side through a high-speed RS485 interface.

The Butterworth filers LPF*n* are specially designed for the control scheme. Take the $i^n_{dq,\mathrm{mea}}$ at rated operation as an example. Assume that the measured phase currents can perfectly track the reference, then ac components in $i^5_{q,\mathrm{mea}}$ and $i^7_{q,\mathrm{mea}}$ appear with a frequency of $6k_0\omega_r$ and amplitudes of about 20 A. These ac components may cause disturbances in their control loops. In order to suppress the ac components, meanwhile, to keep the loops convergent, LPF5 and LPF7 are designed as second-order filters with a cutoff frequency of $0.42k_0\omega_r$, so that the ac components can be attenuated by a factor of 200. The ac component in $i^1_{q,\mathrm{mea}}$ appears with a very small amplitude of 0.67 A and hardly disturbs the control loop, so LPF1 is designed as a first-order filter with a great cutoff frequency of $6k_0\omega_N$, so that a good dynamic is achieved by the loop. Driving the motor under the proposed strategy, phase A currents are measured under a low speed of $0.1\omega_N$ and a high speed of $1.0\omega_N$. Fig. 17 shows the results, which indicate that the reference currents can be tracked precisely under the control scheme.

Since LPF*n* cannot perfectly decouple the currents of different frames in a torque transient process, significant torque pulsations will be caused by interactions of the current loops, as the torque response measured in Fig. 18 shows. In the measurement, $T_{e,\mathrm{cmd}}$ is given as a step from 0 to T_N. To suppress the pulsations, a loop switch is used, which disables the fifth and seventh loops at beginning of the step, and then enables the loops again when outputs of LPF5 and LPF7 become stable. Torque response with the loop switch is measured in Fig. 18, which shows that the torque pulsations are effectively suppressed. A good dynamic performance of the electromagnetic torque is realized.

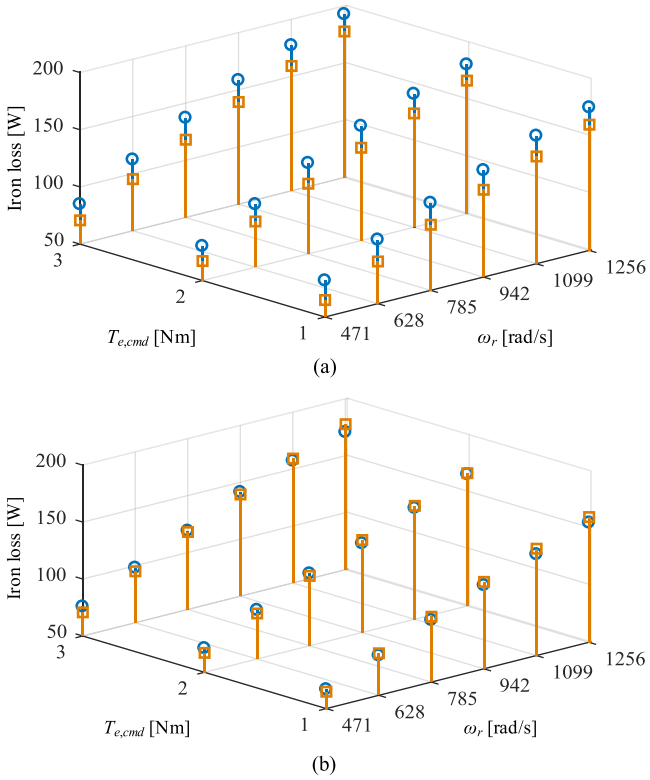

Fig. 19. Measured stator iron loss under various load commands and speeds (a) with and (b) without PWM pulsations of the airgap field. The measured and calculated results are marked with circular and square symbols, respectively.

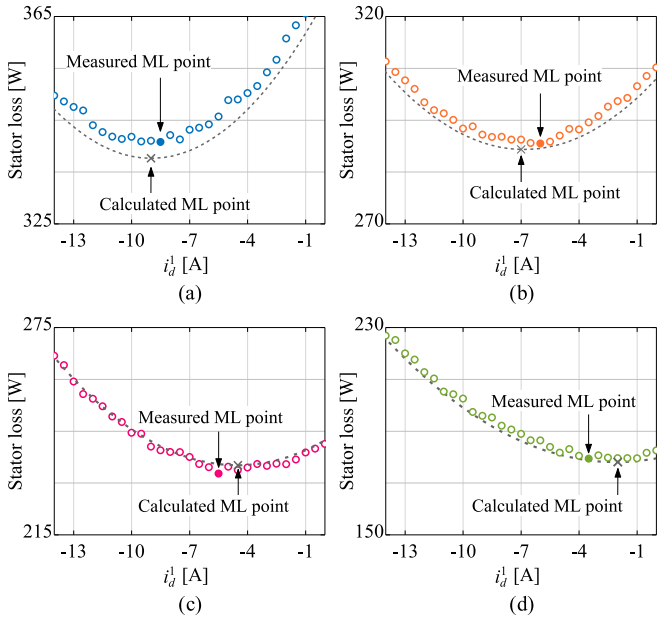

Fig. 20. Behaviors of total stator loss versus i_d^1 measured under the rated load and different rotor speeds of (a) $1.00\omega_N$, (b) $0.75\omega_N$, (c) $0.50\omega_N$, and (d) $0.25\omega_N$.

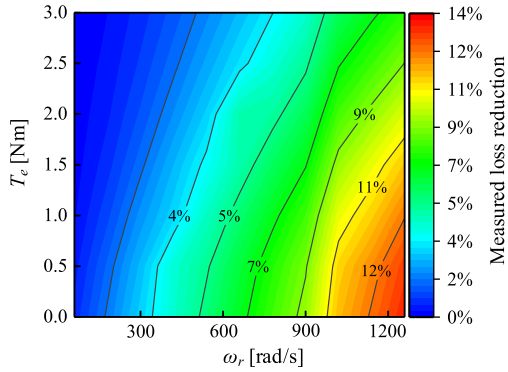

Fig. 21. Measured stator loss reduction of the proposed strategy with respect to CLM strategy mapped in full operation range of the motor.

B. Iron Loss Precision Validation

In the test, the motor is driven under the proposed strategy. Stator iron losses under various load commands and speeds are measured by subtracting the output power and copper loss from the active input power of the motor. Some friction losses are included in the measured iron loss, but they are small enough to be ignored. Fig. 19(a) presents the measured results, compared with the results calculated from a union of (26), (15), and (16). It is seen that the measured results are generally greater than the calculated ones. The reason may be that the airgap field pulsation, which is caused by SVPWM, results in additional hysteresis loss and eddy-current loss in the stator core [24]. According to the study in [25], the additional loss can be removed from the measured input power if PWM carrier harmonics of the phase voltage are filtered. In the test, a LPF is realized by WT3000 with a cutoff frequency of 15 kHz. The stator iron losses are remeasured as shown in Fig. 19(b), which have a good agreement with the calculated results. Therefore, the iron loss evaluation based on the new model of NS-PMSM is validated to be precise without PWM pulsations of the airgap field.

C. Proposed Strategy Validation

Given $T_{e,\mathrm{cmd}} = T_N$, $\omega_r = 1.00\omega_N$, $0.75\omega_N$, $0.50\omega_N$, and $0.25\omega_N$, the total stator loss are measured under various i_d^i. Other i_d^n and i_q^n are determined by the constraints (24a) and (24b). Fig. 20 shows the measured results compared with the calculated ones. It is indicated that the proposed strategy can accurately track the ML points under different rotor speeds.

Stator loss reduction of the proposed strategy with respect to CLM strategy is measured in full operation range of the motor and mapped in Fig. 21. The difference in motor efficiency between the two strategies are mapped in Fig. 22. As can be seen, the measured loss reductions roughly agree with the theoretical results of Fig. 11. The greatest reduction comes to about 12% under rated speed and light load, resulting in a 2.1% enhancement of the motor efficiency. In the rated speed and load, the stator loss can be reduced by 9%, and the efficiency is enhanced by 0.7%, from 90.5% under CLM to 91.2% under the proposed strategy.

The electromagnetic torque error is defined as $(1 - T_e/T_{e,\mathrm{cmd}})$. Fig. 23 shows the measured errors under various rotor speeds and load commands. It is seen that for CLM strategy,

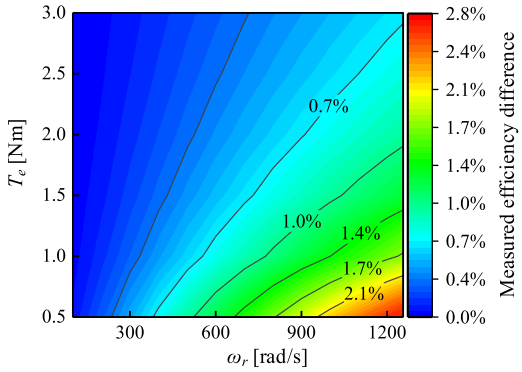

Fig. 22. Measured difference in motor efficiency between the proposed and CLM strategies mapped in full operation range of the motor.

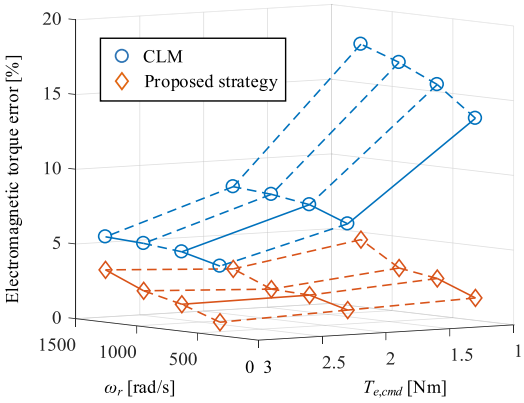

Fig. 23. Electromagnetic torque errors measured for the proposed and CLM strategies under various rotor speeds and load commands.

the errors get greater with $T_{e,\mathrm{cmd}}$ decreasing and ω_r increasing. Especially in the operation of $T_{e,\mathrm{cmd}} = 1.0$ N·m and $\omega_r = \omega_N$, the error comes to as great as 18%. By contrast, since the iron loss torque has been compensated by the proposed strategy, the torque errors are suppressed to a very small level of 5% in full operation range of the motor.

Instantaneous feedback currents $i^n_{q,fdb}$ and the corresponding electromagnetic torque T_e are measured under the proposed strategy in a lower dc supply of 240 V. The motor is operated under torque control model by default. Other conditions are $pf_N = 0.216$ V/(rad/s), $T_{e,\mathrm{des}} = T_N$. The load proportional coefficient is selected as T_N/ω_N, that means the motor will run to rated speed if the dc supply is unlimited. Fig. 24 ranging from 250 to 300 ms shows the measured results without considering the finite dc supply. It is seen that the feedback currents cannot track the reference $i^n_{q,\mathrm{opt}}$ precisely, resulting in a significant torque ripple. The average speed and stator loss are measured as 1172.9 rad/s and 287.3 W. Fig. 24 ranging from 300 to 350 ms shows the measured results considering the finite dc supply. The motor is driven in speed control mode with the reference of 1110.9 rad/s, and $T_{e,\mathrm{cmd}}$ is regulated to 2.65 N·m to match the load adaptively. It is seen that the feedback currents track well with the references, and the electromagnetic torque is produced

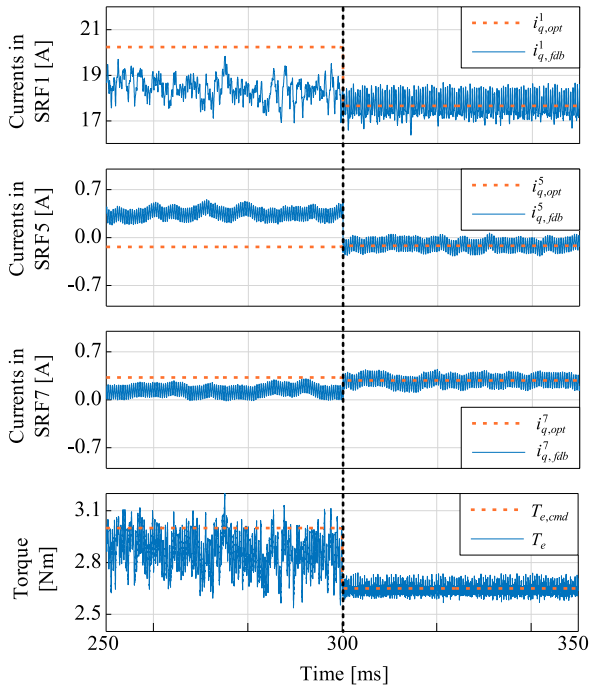

Fig. 24. Measured instantaneous feedback currents and electromagnetic torque with and without considering the finite dc supply voltage. AC components included in source data of $i^n_{q,fdb}$ are further attenuated offline to make the comparisons more clear.

TABLE I
TESTED E_{rrl} UNDER VARIOUS K_6 AND OPERATIONS

$T_{e,cmd}$	ω_r	k_6=1.3	k_6=1.5
$0.17T_N$	$0.33\omega_N$	0.1%	0.6%
	$0.66\omega_N$	0.5%	1.3%
	$1.00\omega_N$	1.1%	2.0%
$1.00T_N$	$0.33\omega_N$	0.0	0.1%
	$0.66\omega_N$	0.1%	0.5%
	$1.00\omega_N$	0.4%	0.9%

with a very small ripple. The stator loss is measured as 281.5 W, which agrees with the result of 279.6 W measured under the same speed and $T_{e,\mathrm{cmd}}$ but a higher dc supply of 290 V. Above measurement indicates that the proposed strategy has a good performance in maintaining the loss-minimization operation under finite dc supply voltage.

In order to validate robustness of the proposed strategy to phase resistance variation, the loss control error E_{rrl} is measured under various k_6 and operations. The dc supply voltage is given as 290 V. The results are listed in Table I. It is seen that E_{rrl} becomes greater when the phase resistance increases during the operation. The greatest E_{rrl} is measured as only 2.0% in an operation with high speed of $1.00\omega_N$ and low load command of $0.17T_N$. It is validated that the proposed strategy characterizes a good robustness to phase resistance variation.

TABLE II
TESTED STATOR LOSSES OF TWO STRATEGIES

	$P_{s,SRF1}$ (W)	$P_{s,opt}$ (W)	$P_{s,SRF1} - P_{s,opt}$ (W)
$0.25\omega_N$	184.1	179.5	4.6
$0.50\omega_N$	240.6	233.7	6.9
$0.75\omega_N$	299.6	290.3	9.3
$1.00\omega_N$	353.4	341.5	11.9

D. Comparison With Model-Based Strategy in SRF1

If ignoring the differential items in (4), optimal $i_{d,q}$ can be solved according to the optimizing problem described in (6). Transferring the optimal $i_{d,q}$ to $i^n_{d,q}$ in MSRF and then feeding to the current control loop as references, the stator loss under the model-based strategy in SRF1 can be tested. Given $T_{e,\mathrm{cmd}}$ as T_N, Table II lists the test results $P_{s,\mathrm{SRF1}}$ under various rotor speeds, compared with the results $P_{s,\mathrm{opt}}$ of the proposed strategy. It is seen that the strategy in SRF1 produces a greater stator loss than the proposed strategy because the iron loss evaluated in SRF1 mismatches with the physical view. In a higher speed, loss difference $(P_{s,\mathrm{SRF1}} - P_{s,\mathrm{opt}})$ between the two strategies becomes more significant.

V. CONCLUSION

In this article, a new model of NS-PMSM has been developed under a combination of the theories of MSRF and iron loss resistance. Based on the model, the stator iron loss has been evaluated precisely and matched well with the physical view. A loss-minimization strategy has been proposed for NS-PMSM, with an improvement of more efficient implementation compared to traditional search strategy. Precise iron loss evaluation and electromagnetic torque generation have been validated experimentally based on a 3.8-kW NS-PMSM. Compared to the CLM strategy, loss reductions of 9% and efficiency enhancement of 0.7% have been observed at rated operation of the motor.

APPENDIX

3.8-KW NS-PMSM SPECIFICATIONS

Rated speed	ω_N	1256 rad/s
Rated torque	T_N	3.0 Nm
Phase resistance	R	0.323 Ω (25℃)
Phase inductance	L	1.2 mH
Number of pole pairs	k_0	2
Iron loss resistance in SRF1	R_i	185 Ω under ω_N
Other parameters in MSRF		
	e_q^1	0.1554 V/(rad/s)
	e_q^5	-0.0025 V/(rad/s)
	e_q^7	-0.0061 V/(rad/s)
	a	0.0656 Ω/(rad/s)
	b	13.46 Ω

ACKNOWLEDGMENT

The article has not been presented at a conference or submitted elsewhere previously.

REFERENCES

[1] E. M. Tsampouris, M. E. Beniakar, and A. G. Kladas, "Geometry optimization of PMSMs comparing full and fractional pitch winding configurations for aerospace actuation applications," *IEEE Trans. Magn.*, vol. 48, no. 2, pp. 943–946, Feb. 2012.

[2] H. Guo, J. Xu, and Y. Chen, "Robust control of fault-tolerant permanent-magnet synchronous motor for aerospace application with guaranteed fault switch process," *IEEE Trans. Ind. Electron.*, vol. 62, no. 12, pp. 7309–7321, Dec. 2015.

[3] M. Chou and C. Liaw, "PMSM-driven satellite reaction wheel system with adjustable DC-link voltage," *IEEE Trans. Aerosp. Electron. Syst.*, vol. 50, no. 2, pp. 1359–1373, Apr. 2014.

[4] R. Ni, D. Xu, and L. Qu, "Maximum efficiency per ampere control of permanent-magnet synchronous machines," *IEEE Trans. Ind. Electron.*, vol. 62, no. 4, pp. 2135–2143, Apr. 2015.

[5] N. Urasaki, T. Senjyu, and K. Uezato, "Relationship of parallel model and series model for permanent mag net synchronous motors taking iron loss into account," *IEEE Trans. Energy Convers.*, vol. 19, no. 2, pp. 265–270, Jun. 2004.

[6] W. Xie, X. Wang, and D. Gerling, "Dynamic loss minimization of finite control set-model predictive torque control for electric drive system," *IEEE Trans. Power Electron.*, vol. 31, no. 1, pp. 849–860, Jan. 2016.

[7] S. Yamamoto, H. Hirahara, and K. Matsuse, "Maximum efficiency drives of synchronous reluctance motors by a novel loss minimization controller with inductance estimator," *IEEE Trans. Ind. Appl.*, vol. 49, no. 6, pp. 2543–2551, Nov./Dec. 2013.

[8] M. N. Uddin and F. Azevedo, "Online loss-minimization-based adaptive flux observer for direct torque and flux control of PMSM drive," *IEEE Trans. Ind. Appl.*, vol. 52, no. 1, pp. 425–431, Jan. 2016.

[9] Z. Q. Zhu, J. H. Leong, and X. Liu, "Control of stator torsional vibration in PM brushless AC drives due to non-sinusoidal back-EMF and cogging torque by improved direct torque control," in *Proc. Int. Conf. Elect. Mach. Syst.*, Beijing, China, 2011, pp. 1–6.

[10] H. Flieh, R. D. Lorenz, and Y. Nakamura, "Dynamic loss minimizing control of a permanent magnet servomotor operating even at the voltage limit when using Deadbeat-Direct torque and flux control," *IEEE Trans. Ind. Appl.*, vol. 55, no. 3, pp. 2710–2720, May/Jun. 2019.

[11] J. Lee, K. Nam, and S. Kwon, "Loss-minimizing control of PMSM with the use of polynomial approximations," *IEEE Trans. Power Electron.*, vol. 24, no. 4, pp. 1071–1082, Apr. 2009.

[12] G. Buja, M. Bertoluzzo, and R. K. Keshri, "Torque ripple-free operation of PM BLDC drives with petal-wave current supply," *IEEE Trans. Ind. Electron.*, vol. 62, no. 7, pp. 4034–4043, Jul. 2015.

[13] G. Feng, C. Lai, and N. C. Kar, "An analytical solution to optimal stator current design for PMSM torque ripple minimization with minimal machine losses," *IEEE Trans. Ind. Electron.*, vol. 64, no. 10, pp. 7655–7665, Oct. 2017.

[14] P. Kshirsagar and R. Krishnan, "High-efficiency current excitation strategy for variable-speed nonsinusoidal back-EMF PMSM machines," *IEEE Trans. Ind. Appl.*, vol. 48, no. 6, pp. 1875–1889, Nov. 2012.

[15] H. Zhang, M. Dou, and L. Yan, "Effects of stator iron loss and current-loop delay on copper-loss-minimizing torque control of BLDCM: Analysis and improvements," *IEEE Trans. Power Electron.*, vol. 34, no. 6, pp. 5620–5631, Jun. 2019.

[16] A. Ruf, S. Steentjes, and K. Hameyer, "Stator current vector determination under consideration of local iron loss distribution for partial load operation of PMSM," *IEEE Trans. Ind. Appl.*, vol. 52, no. 4, pp. 3005–3012, Jul./Aug. 2016.

[17] A. Frias, A. Kedous-Lebouc, and O. Messal, "Loss minimization of an electrical vehicle machine considering its control and iron losses," *IEEE Trans. Magn.*, vol. 52, no. 5, May 2016, Art. no. 8102904.

[18] A. H. Abosh, Z. Q. Zhu, and Y. Ren, "Reduction of torque and flux ripples in space vector modulation-based direct torque control of asymmetric permanent magnet synchronous machine," *IEEE Trans. Power Electron.*, vol. 32, no. 4, pp. 2976–2986, Apr. 2017.

[19] G. Liu, B. Chen, K. Wang, and X. Song, "Selective current harmonic suppression for high-speed PMSM based on high-precision harmonic detection method," *IEEE Trans. Ind. Informat.*, vol. 15, no. 6, pp. 3457–3468, Jun. 2019.

[20] D. Lin, P. Zhou, and Z. J. Cendes, "The effects of steel lamination core losses on 3D transient magnetic fields," *IEEE Trans. Magn.*, vol. 46, no. 8, pp. 3539–3542, Aug. 2010.

[21] G. Bramerdorfer and D. Andessner, "Accurate and easy-to-obtain iron loss model for electric machine design," *IEEE Trans. Ind. Electron.*, vol. 64, no. 3, pp. 2530–2537, Mar. 2017.

[22] H. Ge, B. Bilgin, and A. Emadi, "Global loss minimization control of PMSM considering cross-coupling and saturation," in *Proc. IEEE Energy Convers. Congr. Expo.*, Montreal, QC, Canada, 2015, pp. 6139–6144.
[23] S. Yamamoto, H. Hirahara, and A. Tanaka, "Universal sensorless vector control of induction and permanent-magnet synchronous motors considering equivalent iron loss resistance," *IEEE Trans. Ind. Appl.*, vol. 51, no. 2, pp. 1259–1267, Mar./Apr. 2015.
[24] Y. Miyama and M. Inoue, "PWM carrier harmonic iron loss reduction technique of permanent-magnet motors for electric vehicles," *IEEE Trans. Ind. Appl.*, vol. 52, no. 4, pp. 2865–2871, Jul./Aug. 2016.
[25] A. Boglietti, A. Cavagnino, and M. Pastorelli, "Predicting iron losses in soft magnetic materials with arbitrary voltage supply: An engineering approach," *IEEE Trans. Magn.*, vol. 39, no. 2, pp. 981–989, Mar. 2003.

Haitao Zhang was born in Shanxi, China, in 1988. He received the B.S. and M.S. degrees in electrical engineering from Northwestern Polytechnical University, Xi'an, China, in 2009 and 2012, respectively, where he is currently working toward the Ph.D. degree in electrical engineering.

From 2012 to 2015, he was a Software Engineer with Bosch Rexroth, Xi'an. His research interests include optimal control and design of permanent magnet motors.

Manfeng Dou (Member, IEEE) received the M.S. and Ph.D. degrees in electrical engineering from Northwestern Polytechnical University (NPU), Xi'an, China, in 1991 and 1998, respectively.

He is currently a Professor with NPU and the Vice-Director of the Institute of Rare Earth Permanent Magnet Electric Machine and Control Technology, NPU. His research interests include electrical machine design, analysis of electromagnetic fields, motion control technology, and intelligent control.

Dr. Dou was a recipient of the second prize for the China National Invention Award in 1993, the second prize for the China National Defense Science and Technology Progress Award in 2007, and the Youth Science Award of Shaanxi Province, China, in 2004.

Jia Deng was born in Henan, China, in 1995. He received the B.S. degree in electrical engineering from Northwestern Polytechnical University, Xi'an, China, in 2018, where he is currently working toward the master's degree.

His research interests include optimal control and design of permanent magnet synchronous motor used in high performance industrial applications.